doi:10.1016/j.jmb.2008.06.037 J. Mol. Biol. (2008) 381, 1168–1183

JMB

Available online at www.sciencedirect.com

ScienceDirect

ELSEVIER

Cholesterol Effects on BAX Pore Activation

Eric Christenson, Sean Merlin, Mitsu Saito and Paul Schlesinger*

Department of Cell Biology and Physiology, Washington University School of Medicine, St. Louis, MO 63110, USA

Received 13 February 2008; received in revised form 11 June 2008; accepted 13 June 2008
Available online
20 June 2008

The importance of BCL-2 family proteins in the control of cell death has been clearly established. One of the key members of this family, BAX, has soluble, membrane-bound, and membrane-integrated forms that are central to the regulation of apoptosis. Using purified monomeric human BAX, defined liposomes, and isolated human mitochondria, we have characterized the soluble to membrane transition and pore formation by this protein. For the purified protein, activation, but not oligomerization, is required for membrane binding. The transition to the membrane environment includes a binding step that is reversible and distinct from the membrane integration step. Oligomerization and pore activation occur after the membrane integration. In cells, BAX targets several intracellular membranes but notably does not target the plasma membrane while initiating apoptosis. When cholesterol was added to either the liposome bilayer or mitochondrial membranes, we observed increased binding but markedly reduced integration of BAX into both membranes. This cholesterol inhibition of membrane integration accounts for the reduction of BAX pore activation in liposomes and mitochondrial membranes. Our results indicate that the presence of cholesterol in membranes inhibits the pore-forming activity of BAX by reducing the ability of BAX to transition from a membrane-associated protein to a membrane-integral protein.

Keywords: apoptosis; BCL-2 family; protein–membrane interactions; pore formation; cholesterol

Edited by J. Bowie

Introduction

Genetically programmed apoptotic cell death occurs in all multicellular organisms.[1] Control of the death decision prominently involves a three-part regulatory ensemble of proteins, the BCL-2 family.[2] Twenty-five genes comprise this family and they generate three functional classes of proteins: proapoptotic and antiapoptotic actors with a supporting cast of BH3-only proteins that modulate their interaction.[3,4] To function as the apoptotic decision agent, these proteins collaborate to form a gateway, "pore", in the outer mitochondrial membrane (OMM).[5–7] The formation of this pore requires the availability of active and uninhibited BAK or BAX in the OMM.[8] BAX and many of the other proteins are soluble and move to the mitochondrial outer membrane in concert with the death signaling.[9,10] Others have demonstrated the formation of BAX homo-oligomers in mitochondria and inferred a correlation with a mortality decision in the OMM.[11–14] However, the nature of the BCL-2 family protein interactions while in membranes is not clear. Furthermore, the molecular events and environmental conditions that trigger BAX transformation to an active state have remained elusive. Recent studies have indicated that suppression of BAX inhibition is critical in the mortality decision.[15–17] While it is possible that negative regulation is a dominant theme in apoptosis, this gives no explanation of the mechanism by which BAX becomes situated in the OMMs and is availed of the negative regulation. Furthermore, if the regulation is entirely negative by antiapoptotic BCL-2 family members in the OMM, then the escape of the remaining and vastly larger membrane surface of the cell from BAX predation is a mystery.

Both pore-forming and regulatory interactions of BCL-2 family proteins occur at the mitochondrial

*Corresponding author. E-mail address: paul@cellbio.wustl.edu.

Abbreviations used: TMPD, *N*,*N*,*N*,*N*-tetramethyl-*p*-phenylenediamine; *ent*-cholesterol, full enantiomer of cholesterol; DOPC, dioleoylphosphatidylcholine; DOPA, dioleoylphosphatidic acid; OMM, outer mitochondrial membrane; CF, carboxyfluorescein; fM, fused mitochondria; EGTA, ethylene glycol bis(β-aminoethyl ether)*N*,*N*′-tetraacetic acid; VDAC, voltage-dependent anion-selective channel; OG, *n*-octyl-β-D-glucopyranoside.

outer membrane. Previously, we have shown that one proapoptotic protein, genetically engineered active BAX [BAX(ΔC19)], can form large pores in planar lipid bilayers.[18] Subsequently, we characterized these pores in defined liposomes as consisting of dimers and tetramers of BAX(ΔC19). The tetrameric pore was able to accommodate cytochrome *c* for release from the liposome.[19] From the kinetics of pore activation upon addition of soluble monomeric BAX(ΔC19), we concluded that the oligomerization into pores occurred after membrane insertion and postulated that it would be dependent upon the membrane environment. Therefore, we have undertaken studies to explore the role of membrane lipids on BCL-2 family protein pore activation.

In these studies, we have determined the BAX(ΔC19) pore activation in the presence of cholesterol and the enantiomer of cholesterol.[20] Cholesterol is necessary for membrane function in eukaryotic cells, but the chemical and physical basis for the cholesterol requirement remains unclear.[21] Cholesterol is synthesized in the endoplasmic reticulum and is internalized with the plasma membrane and by receptor-mediated endocytosis. From both the endoplasmic reticulum and the late endosomal pathway, cholesterol enters other compartments of the cell.[22] In steroidogenic tissues, for example, adrenal and placenta, hormone production is initiated by side-chain cleavage in the mitochondrial matrix.[23,24] In other cells, mitochondrial cholesterol oxidation occurs at lower rates but can become pathogenic when the cells are cholesterol overloaded.[25] When cholesterol is taken up by mitochondria, it first resides in the OMM and is then transferred through the contact sites using the peripheral benzodiazepine receptor to the matrix for oxidation.[26,27] It has been suggested that movement of cholesterol from the OMM to the inner mitochondrial membrane, where oxidation occurs, is facilitated by a cholesterol recognition/interaction amino acid consensus motif that is observed in the peripheral benzodiazepine receptor.[28] In mammalian cells, the plasma membrane has the highest cholesterol content but significant cholesterol, oxysterols, and bile acids are found in the mitochondria because of the matrix oxidative production of these steroids.[29,30] Cholesterol has been reported to be elevated in cultured tumor cells.[31,32] Recently, bilayer cholesterol content has been shown to influence BAX oligomerization and trypsin resistance in liposomes and mitochondria.[33] Others have reported complex relationships among lipids, cholesterol, BAX, and permeability transition pore activation.[34] These observations have been used to explain the effects of cholesterol upon cellular apoptosis. We have studied the effect of cholesterol on BAX pore formation in liposomes and mitochondria and conclude that the cholesterol content of the plasma membrane protects it from the pore formation when BAX is activated. In particular, the addition of cholesterol to the outer membrane of mitochondria inhibits pore formation by BAX. We discuss the mechanism of cholesterol inhibition of BAX pore activation in terms of membrane binding and integration and speculate on how this might influence apoptosis in mammalian cells.

Results

Although the BCL-2 family proteins are clearly the arbiters of a mortality decision, the biochemical steps that conclude in the mitochondrial death decision are not yet clear. We have pursued a reconstitution methodology to study these phenomena in order to clearly define the biochemical and biophysical processes in the reaction steps leading to the initiation of apoptosis. Initially, these studies revealed that a genetically engineered form of active BAX, BAX(ΔC19), could form a cytochrome *c* competent pore in liposomes.[19] Hill analysis revealed that in liposomes, active BAX(ΔC19) inserted into the membrane as a monomer formed a functioning pore as a dimer and displayed a concentration-dependent progression to a tetramer complex that transferred cytochrome *c* out of the liposomes. We are revisiting this method of analysis in order to study the effects of lipid environment on BAX membrane integration and pore formation.

Human BAX expression, purification, and studies of pore activation

Native BAX in mammalian cells is a soluble protein that must be activated to induce apoptosis.[3,35] This protein can be activated *in vitro* in several ways. In this study, we have used a genetically engineered form of active human BAX, BAX(ΔC19), which has a portion of the α-helix 9 removed. In 0.1% *n*-octylglucoside, this form of human BAX(ΔC19) is monomeric with a molecular weight of 19,000±1200 as determined by dynamic light scattering and by SDS-PAGE (Fig. 1a). In these studies, we used the human BAX(ΔC19) because we would employ human mitochondria to study pore formation in these organelles. The pore activation and stoichiometry of human BAX(ΔC19) have not been previously reported. The human and mouse BAX proteins are very similar in sequence but arginine 64 in the critical BH3 region is replaced with a lysine. In addition, there is a rearrangement of the prolines adjacent to the first α-helix (residues 46–53). Proteolytic cleavage and phosphorylation in this region of BAX influence the mitochondrial translocation and pore formation.[36,37]

We concluded that confirmation of a similar mechanism of pore formation by the human protein was warranted. Using liposomes loaded with carboxyfluorescein (CF) at quenching concentrations, we studied the activation of pores by human BAX(ΔC19) (Fig. 1b). The time-series data normalized to the total dequenching for each preparation of liposomes are an exponential release. This is consistent with a single pore producing full dequenching from a liposome and the exponential time course representing pore activation in the liposomes. The measured time constants were used in a Hill ana-

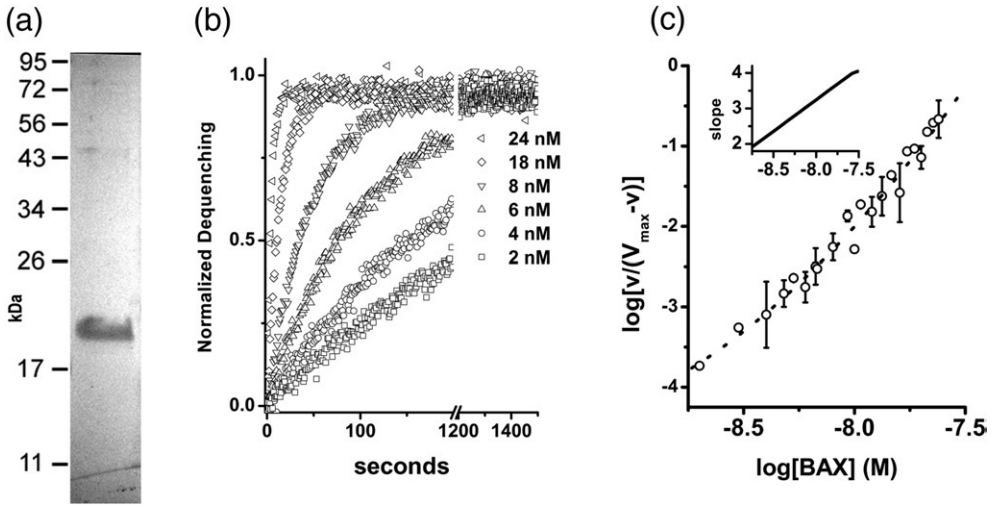

Fig. 1. Human BAX(ΔC19) pore-forming activity in liposomes. Using human BAX(ΔC19), we studied the kinetics of pore activation in liposomes by the purified protein. The liposome assay was done as previously described.[19] (a) Preparation of human BAX(ΔC19) expressed and purified as described in Materials and Methods and run on SDS-PAGE gel to demonstrate size and purity. (b) Time-series examples of human BAX(ΔC19) pore activation as added protein concentration is increased. The following BAX(ΔC19) concentrations are shown: ◁, 24 nM; ○, 18 nM; △, 8 nM; ▽, 6 nM; ◊, 4 nM; □, 2 nM. Using the time-series data curve fitting to an exponential function, we determined the time constant and the extent of release. (c) The time constants determined from the time series and concentration dependence of pore activation were subjected to Hill analysis. Each plotted point represents the average of two to three determinations with standard deviations shown when they were bigger than the symbol. The data were fitted to a polynomial using the Levenberg–Marquardt algorithm. The slope of the fitted line was determined at each point and is plotted in the inset graph.

lysis of the human BAX(ΔC19) pore activation (Fig. 1c). The concentration dependence of human BAX(ΔC19) activation in liposomes indicates a pore activation stoichiometry of 2 and 4, similar to the previously published model for the murine protein.[19]

A mitochondrial preparation for the study of OMM permeability

The permeability of the OMM is a key factor in the apoptosis death decision.[38] These studies have used HeLa cell mitochondria and human BAX protein. We have adapted the fusion of liposomes with purified mitochondria to create a preparation for the study of OMM permeability.[39,40] The unfused liposomes were removed by low-speed pelleting of the resulting mitochondria. The fused mitochondria (fM) have a normal double-membrane morphology (Fig. 2a). The captured CF produced photoconversion of diaminobenzidine and electron-dense deposition in the intermembrane space (Fig. 2a, photoconverted). CF containing mitochondria and liposomes were identified by this method, but the insoluble photoconversion product obscures the membranes.[41,42]

Cytochrome *c*-dependent oxygen consumption can be used to evaluate the continuity of the OMM.[43] When our preparation was studied using a Clark electrode to determine site IV-dependent oxygen consumption in the presence of saturating substrate and oxygen, they consumed 43.1±0.4 nAtom mg^{-1} min^{-1}, which is similar to that of rat liver mitochondria (48.5±0.4 nAtom mg^{-1} min^{-1}) but less than that of skeletal muscle or kidney mitochondria.[44] This rate of oxygen uptake suggests that in the preparation, the OMM is intact and cytochrome *c* is retained within the intermembrane space. Using the membrane-active peptide melittin, we interrupted the uptake of oxygen by the mitochondria as shown in Fig. 2b. This reduction is reversed by the addition of 100 μM horse cytochrome *c* to the electrode chamber. The oxygen consumption in these preparations is dependent upon ADP and phosphate and is sensitive to azide. We conclude that our isolated mitochondria have an intact OMM and that cytochrome *c* is retained during the isolation procedure.

Ca^{2+} dependence of fM permeability

The fM preparation was performed in media containing ethylene glycol bis(β-aminoethyl ether) *N*,*N*′-tetraacetic acid (EGTA) so that Ca^{2+} concentration is less than 10 nM. At this low calcium concentration, the CF is retained within the OMM barrier. Increasing the media calcium to 100 or 200 μM initiated rapid dequenching of the CF from the intermembrane space (Fig. 2c). Dequenching is normalized to the maximum dequenching produced by 1% Triton X-100. The dequenching is rapid and dependent upon calcium concentration and is consistent with activation of the voltage-dependent anion-selective channel (VDAC) of the OMM.[45]

Presence of porin-like channel activity in the mitochondrial preparation

The release of anionic CF by Ca^{2+} elevation suggests that VDAC is present but in a low conductance

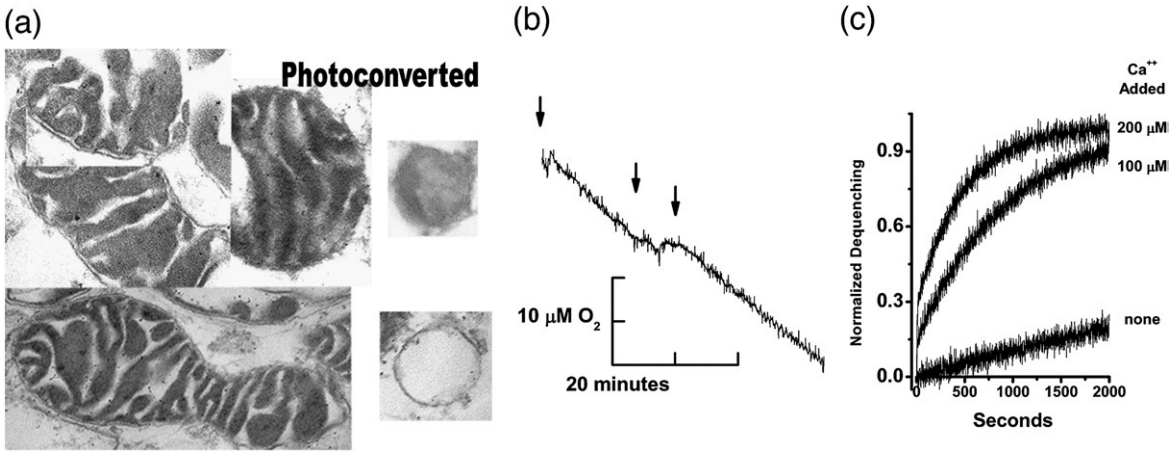

Fig. 2. Studies on isolated mitochondria after fusion with CF liposomes. (a) Mitochondria were prepared and fused with 200 nm liposomes containing 20 mM CF as described in Materials and Methods. These mitochondria were then pelleted, fixed, and embedded for sectioning and electron microscopy. In all cases, the mitochondria have a traditional two-membrane morphology after fusion with liposomes. Exposure of the isolated mitochondria to UV light photoconverted the CF and photooxidized diaminobenzidine, producing the electron-dense depositions in the intermembrane space. Two large unilamellar liposomes that were used in the fusion loading of the mitochondria are seen on the right. The upper liposome was photoconverted and the lower one was not exposed to UV light (see Materials and Methods). (b) After isolation and fusion with liposomes containing CF, the mitochondrial suspension was diluted to 1 mg/ml protein and O_2 consumption was measured. At the first arrow, 10 mM ascorbate and TMPD were added, initiating rapid O_2 uptake that was dependent upon cytochrome *c* and cytochrome oxidase; at the second arrow, 200 nM melittin was added; at the third arrow, 100 μM horse cytochrome *c* was added. (c) Mitochondria were isolated and fused with liposomes as described in Materials and Methods in the presence of 1 mM EGTA. Subsequently, the washed mitochondrial suspension was diluted 1:100 into the assay buffer or buffer added with 100 or 200 μM $CaCl_2$ (from bottom to top), and fluorescence dequenching followed for the indicated times. All dequenching values were normalized to the 1% Triton X-100-initiated dequenching.

state in our fM preparation.[45] We have directly assessed the channel activity of the fM in planar lipid bilayers. Using our preparation of mitochondria that was post-liposome fusion, we allowed these to interact with a planar lipid bilayer. After addition of the fM to the *cis* bilayer chamber, fusion transients were observed within 5 min of continuous stirring. After fusions had occurred, the resulting bilayer currents were studied using a ±60-mV voltage ramp or by voltage steps under voltage clamp (Fig. 3a and b). The ramp current pattern was typical of many studies of VDAC currents in

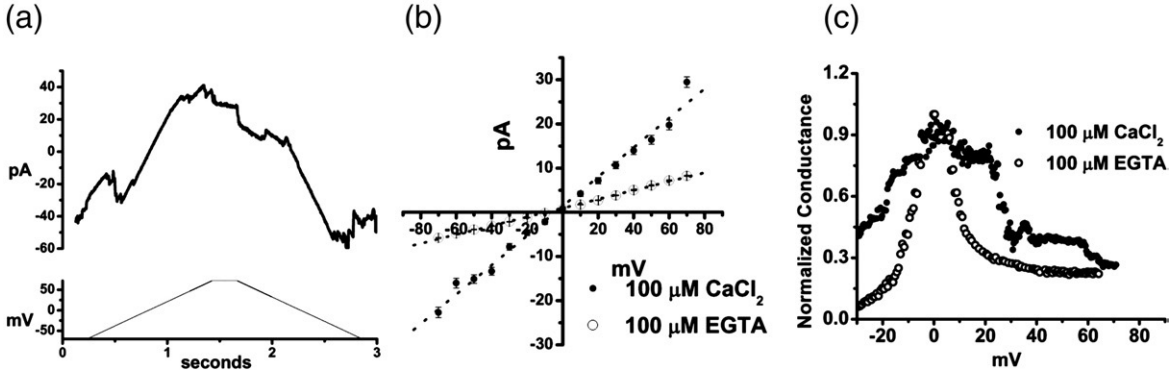

Fig. 3. Channel activity in membranes of liposome–fM. (a) Isolated, liposome–fM from cultured HeLa cells were studied in planar lipid bilayers as described in Materials and Methods. Mitochondria were added to the *cis* chamber of a planar lipid bilayer cuvette with a 450- to 150-mM KCl from the *cis* to *trans* chambers. After 3–7 min, current levels stabilized and the *cis* solution was perfused to 150 mM KCl. Using voltage clamp configuration, command ramps (lower panel) were applied to the bilayer after fusion events were observed. (b) Using buffer containing 100 μM $CaCl_2$ ± 100 μM EGTA, we studied the stable voltage dependence of fM. Data were obtained by holding the indicated membrane potential for 10 s and using the average current of the final 2 s. EGTA (100 μM) was added to the *cis* chamber, and after 5 min, the voltage dependence was determined again. The high-calcium perfusion, voltage dependence, EGTA addition, and voltage dependence redetermination were repeated until the bilayer membrane collapsed (three cycles). These were averaged for this panel, and the standard deviation at each point is shown in the figure. (c) Bilayer conductance was calculated from voltage ramps (±60 mV) collected at 1.67 kHz with a 1.2-s duration for each ramp. The bilayers were formed and Ca^{2+} concentration was adjusted as described in (a). The currents were normalized to a peak conductance of 1 for comparison.

mitochondrial membrane preparations or reconstituted VDAC protein.[46,47] The conductance of these currents was decreased when the Ca^{2+} was reduced with EGTA, consistent with the reported calcium-dependent shift of VDAC to a low conductance channel[45,48] (Fig. 3c). The fM currents also displayed voltage-dependent inactivation as described for the VDACs.[49]

BAX(ΔC19) pore activation in the OMM

Isolated mitochondria used in these studies were loaded with CF by pH-dependent fusion of liposomes with the OMM as described in Materials and Methods. This fusion-mediated transfer effectively loads the mitochondria intermembrane space with CF but at reduced concentration from that present in the liposomes. Therefore, the dequenching response of the mitochondria per mole of lipid is less than that of the primary liposomes. Consequently, in the assay of BAX pore activation using the fM, we have increased the concentration of mitochondria lipid to 4.3 μM, which compensated for the reduced dequenching from the fM preparation. The application of BAX(ΔC19) to this mitochondrial preparation produces a rapid time course of CF dequenching. As shown in Fig. 4a, the kinetics and concentration dependence of BAX(ΔC19)-initiated dequenching from mitochondria are qualitatively consistent with that observed in defined liposomes. There is a distinct difference between specific activity of BAX(ΔC19) pore formation in mitochondria and liposomes. The higher activity of BAX in liposomes can be compensated by correcting for the difference in lipid content in the assay (Fig. 4b). After this adjustment of the rate of pore activation for the increased lipid in the mitochondrial assay, the Hill analysis for pore formation in mitochondria closely resembles what we have observed in liposomes (Fig. 4c). Because of the additional lipid in the mitochondrial assay, the lowest BAX(ΔC19) concentrations (≈1 nM) do not generate sufficient activity for accurate analysis.

Effect of cholesterol on BAX pore activation in defined liposomes

BAX is found in the cytosol of most eukaryotic cells, but when activated in response to proapoptotic stimuli, it becomes integrated into the mitochondrial outer membrane and the endoplasmic reticulum.[50] Because the membranes in which BAX integrates *in vivo* have less cholesterol than the plasma membrane, we have studied the effect of this sterol on interaction of BAX with membranes.

Cholesterol-containing liposomes were prepared and characterized as described in Materials and Methods. The final cholesterol concentration in the liposomes was 20 mol%, and the size of the liposomes was verified by dynamic light scattering. The effect of the cholesterol was to dramatically decrease the BAX(ΔC19) pore activation (Fig. 5a and b). As a consequence, τ values (time constants) were large as was the error in their determination. From these data, we could analyze the Hill plot but not the pore size. Here, we have succeeded in extending the Hill analysis to low enough BAX concentrations that we can discern the curvature in spite of the greater error

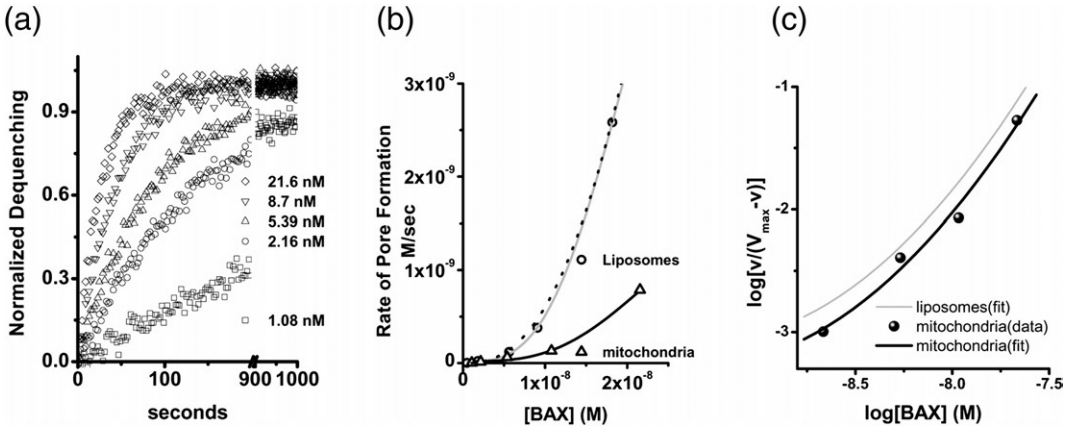

Fig. 4. BAX pore activation in isolated mitochondria. Mitochondria were isolated from cultured HeLa cells and fused with liposomes using a modification of a previously described technique as described in Materials and Methods. (a) Mitochondria were diluted into a 500-μl assay volume to give a protein concentration of 0.3 mg/ml and a phospholipid concentration of 4.3 μM. The concentrations of BAX(ΔC19) are as follows: □, 1.08 nM; ○, 2.16 nM; △, 5.39 nM; ▽, 8.7 nM; ◊, 21.6 nM. The fractional dequenching was fitted to an exponential model in order to determine the time constant (τ) for analysis of the kinetics of BAX pore activation. (b) Comparison of the rate of BAX(ΔC19) pore activation in mitochondria (△) and liposomes (○). Both sets of data are fitted by Hill functions (black and gray lines, respectively). The rate of pore activation in mitochondria was then normalized for the increased lipid in this assay and then was fitted by the dotted black line. The normalized pore activation data points are not shown in this panel. (c) The pore activation time constants that have been normalized for lipid concentration are plotted in the standard logarithmic form for Hill analysis. The data were fitted as in Fig. 1, and the fitted curve was plotted in black. The liposome fitted line is shown in gray for comparison.

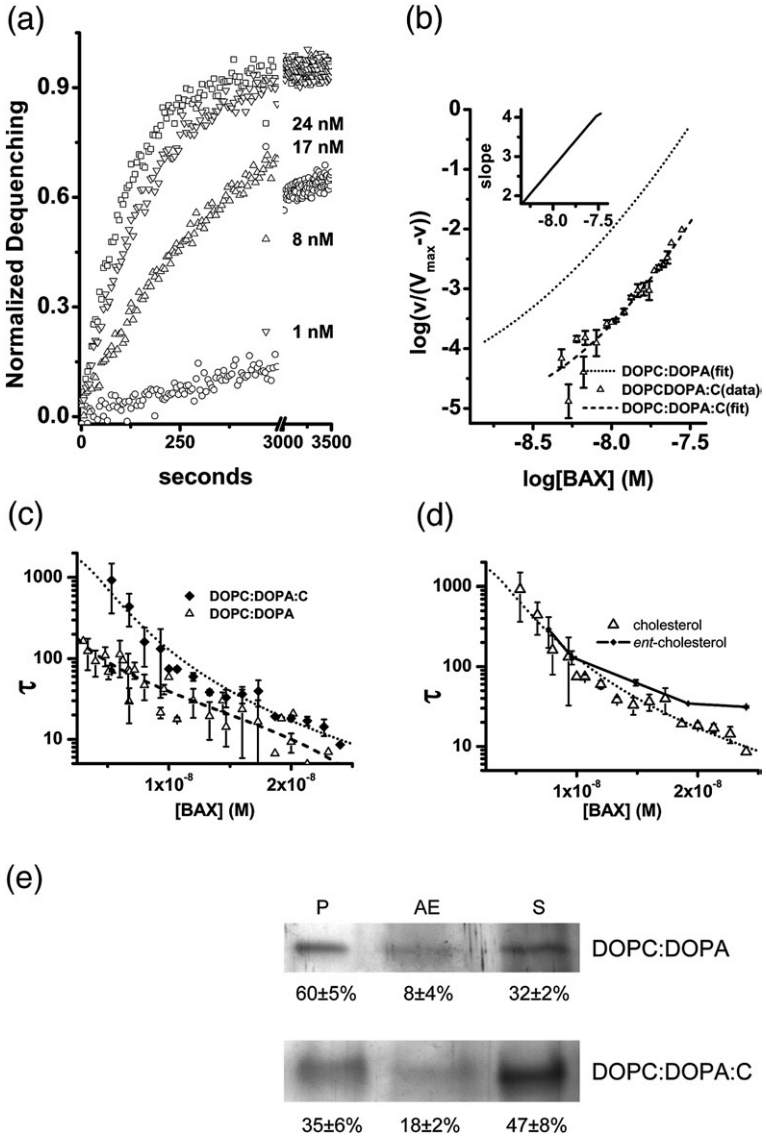

Fig. 5. BAX pore activation and binding in DOPC:DOPA:C liposomes. Liposomes containing cholesterol were prepared as described in Materials and Methods. (a) Selected examples of time-series dequenching by human BAX(ΔC19) in DOPC:DOPA:C (mole fraction, 0.59:0.21:0.20) liposomes. Human BAX(ΔC19) concentrations were as follows: ○, 1 nM; △, 8 nM; ▽, 17 nM; □, 24 nM. Fractional dequenching was computed by comparison with Triton X-100 dequenching. (b) Hill analysis of the human BAX(ΔC19) pore activation in DOPC:DOPA:C liposomes. Each determination of the time constant is shown with the standard deviation error bars ($n \geq 3$). The series of time constants was fitted to a polynomial, and the slope of the fitted line is determined and presented in the inset plot. Also shown is the fitting from Fig. 1c in DOPC:DOPA liposomes, indicated by the dotted line. (c) Comparison of the concentration dependence of the time constant for pore activation in DOPC:DOPA (△) and DOPC:DOPA:C (◆) liposomes. Each of the determinations is shown with standard deviation ($n \geq 3$). Dotted lines are the nonlinear least-squares fitting of the time constants to the Hill equation. (d) Comparison of BAX pore activation in liposomes composed of DOPC:DOPA:C (△) and DOPC:DOPA:*ent*C (mole fraction, 0.59:0.21:0.20) (○). Each of the determinations is shown with standard deviation ($n \geq 3$). Dotted lines are the nonlinear least-squares fitting of the time constants to the Hill equation. (e) Defined liposomes were suspended in 200 nM BAX(ΔC19) and incubated for 10 min at room temperature. As indicated in the figure, the liposomes were ±cholesterol. The liposomes were sedimented at 150,000*g* as described in Materials and Methods to give the pellet (P) and alkaline extraction (AE) or supernatant (S). Each sample was separated by SDS-PAGE with silver staining. The region at 19–20 kDa of the gel was analyzed for density, and the percent distribution of the protein in each fraction was calculated for the figure.

in the measurements of the time constant. When we plot the time constants, the effect of cholesterol is dramatic and increases at lower BAX concentrations (Fig. 5c).

The sterol-mediated inhibition of BAX(ΔC19) pore formation could be due to a direct and stereospecific interaction between steroids and the BAX protein. To test this, we prepared liposomes using the enantiomer of cholesterol. This analog of cholesterol has the configuration inverted at each asymmetric site in the cholesterol molecule.[20] This compound was a generous gift from Dr. D. Covey of the Department of Developmental Biology, Washington University School of Medicine. The comparison of pore activation in liposomes containing *nat*-cholesterol (natural enantiomer of cholesterol) or *ent*-cholesterol (full enantiomer of cholesterol) indicates that the enantiomer is as effective as the natural compound at the inhibition of BAX pore activation (Fig. 5d). This suggested that the effect resulted primarily from cholesterol condensing and other effects upon the lipid membrane environment and not from a stereospecific interaction with BAX.[51–53]

Effect of cholesterol on BAX pore activation in mitochondria

The inhibition of BAX(ΔC19) pore activation by the inclusion of cholesterol in the liposome membrane composition is dramatic. The simple composition of our liposomes might contribute to this inhibition and generate an artificially large inhibition that will not be

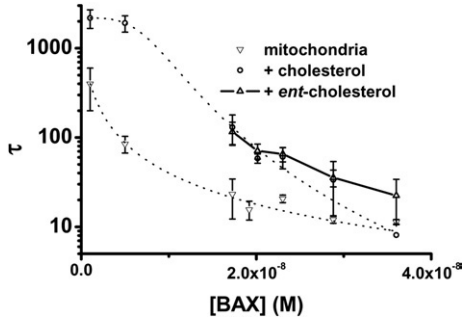

Fig. 6. Effect of sterol on BAX(ΔC19) pore activation in mitochondria. The effect of cholesterol on BAX pore activation in isolated mitochondria fused with liposomes containing 20 mol% cholesterol. Pore activation in these mitochondria (○) was greatly reduced compared to mitochondria fused with DOPC:DOPA liposomes (▽). Mitochondria were also fused with liposomes prepared using the enantiomer of cholesterol (△). The dotted lines are the results of nonlinear least-squares fitting of the time constants for pore activation in mitochondria fused to liposomes and cholesterol liposomes. Time constants of pore activation in mitochondria fused with liposomes prepared with the enantiomer of cholesterol are not fitted.

seen in a more complicated membrane. We wanted to test the effect of cholesterol in a physiologic membrane in which we could alter the composition in a known fashion. Our fM fulfilled these requirements. The native mitochondria supported BAX(ΔC19) pore formation well, and by fusing them with dioleoylphosphatidylcholine (DOPC)/dioleoylphosphatidic acid (DOPA)/C liposomes, we could increase the cholesterol content of the OMM to at least 16 mol% during the fusion step. It has previously been shown that the cholesterol of the OMM is slowly metabolized in isolated mitochondria, indicating that the elevated cholesterol was maintained during our experiments.[23] The addition of cholesterol to OMM produced a substantial inhibition of the pore activation (Fig. 6). However, this reduced the BAX(ΔC19) activity to such an extent that it was not possible for us to characterize the effects on oligomerization and pore size.

BAX interaction with liposome membranes

BAX pore formation requires the translocation of the soluble BAX protein to a bilayer membrane. This

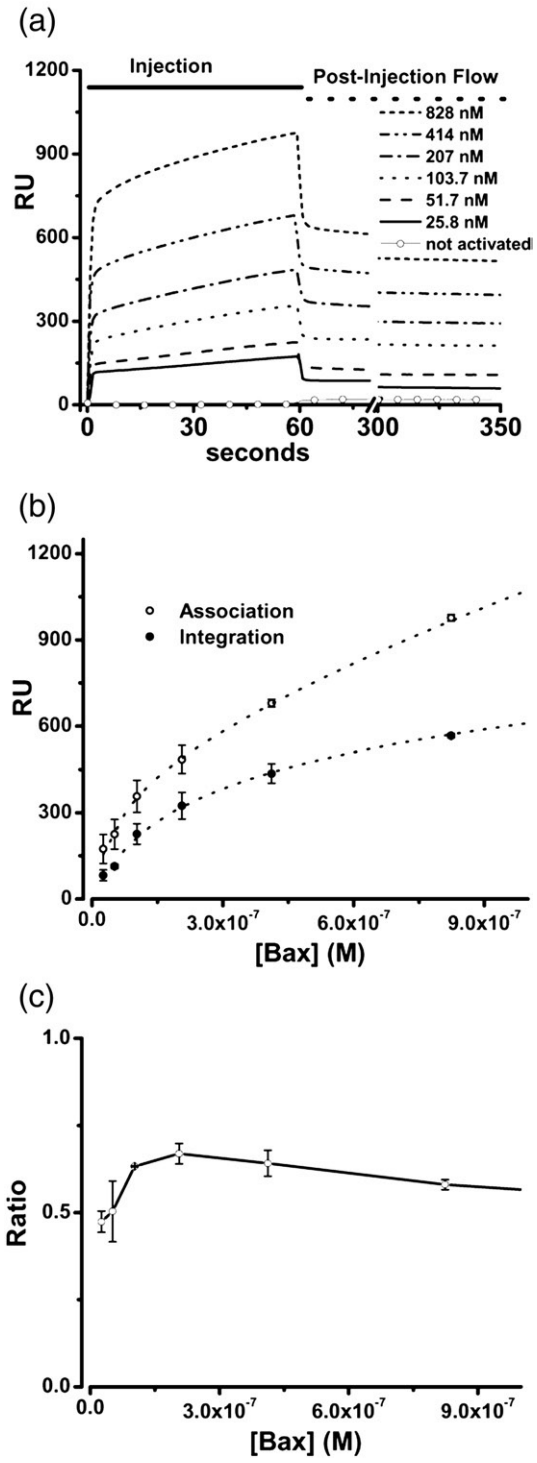

Fig. 7. BAX binding to supported DOPC/DOPA liposomes. The binding and membrane integration of BAX(ΔC19) were studied by surface plasmon resonance using supported liposomes. (a) BAX(ΔC19) was injected over an L1 chip covered with immobilized DOPC/DOPA (74:26 mol%) liposomes as described in Materials and Methods. This protein was prepared as described above without the use of detergent. Prior to exposure of the BAX(ΔC19) to detergent, the protein did not bind to the liposomes as shown by the open circles (○ ○ ○) at the bottom of the graph that indicate the averaged RU response for the 25–3000 nM BAX(ΔC19) concentration range. After treatment with detergent, the RU response for the following concentrations is shown: 25.8 nM (solid), 51.7 nM (dash), 103.7 nM (dot), 207 nM (dash–dot), 414 nM (dash–dot–dot), 828 nM (short dash). The injection phase is indicated by the solid line and the wash phase is denoted by the dashed line at the top of the graph. (b) Comparison of membrane-associated (□) and membrane-integrated (○) protein using the criteria described in the text and calculating the average values and standard deviation as described in Materials and Methods. The dotted lines represent the best fit to an interaction model as described in the text. (c) The ratio of binding and integration fraction of protein plotted as the added concentration of BAX(ΔC19) is increased. Means and standard deviations are computed as described in Materials and Methods.

step is critical *in vivo* and is thought to be a consequence of BAX activation in cells.[36,54,55] The mechanism of the membrane translocation of BAX must progress along a binding followed by an integration model.[56] The progress of translocation will be influenced by contributions from both the protein structure and the membrane environment. The interaction of BAX with membranes can be clearly shown in a defined liposome experimental system (Fig. 5e). Furthermore, the effect of cholesterol appears to be a reduction of membrane-incorporated BAX protein. We have extended the use of defined liposomes to the study of BAX membrane translocation by employing surface plasmon resonance. In this approach, defined liposomes were supported at the sensor surface using the hydrophobic chips (L1) from the Biacore Corporation.[57] With the use of these immobilized liposomes, it was possible to study the interaction of BAX(ΔC19) with the liposome bilayer membrane in concentration- and time-dependent experiments.

For three preparations of activated BAX(ΔC19), the concentration dependence and time course of binding and membrane integration were determined and averaged (Fig. 7a). The membrane-associated BAX populations were characterized by total binding to supported liposome membranes at the end of the injection period (60 s) and the mean stable bound protein after an extended wash period (300–350 s). These populations were determined and are plotted in Fig. 7b as the average of the individual trials along with the fitted lines. The total BAX membrane binding at 60 s was tested against one- and two-state interaction models. A chi-square analysis indicated a two-state model to be preferable with residuals that were reduced 10-fold. The resulting high- and low-affinity estimates for membrane binding are listed in Table 1. The concentration dependence of BAX integration into the liposome membrane was clearly dominated by a single interaction, and the results of that analysis are also presented in Table 1. From this analysis of the binding and integration curves, the size of the membrane populations of BAX was estimated and is presented as mole fractions to correct for small changes in liposome immobilization on the Biacore chip. Inspection of these fitted results for membrane association reveals three populations of membrane-associated BAX: high- and low-affinity populations that rapidly dissociate and the membrane-integrated fraction that slowly dissociates. The ratio of total membrane-bound to membrane-integrated BAX increases at low BAX concentrations and then begins to fall as membrane capacity becomes saturated (Fig. 7c).

BAX interaction with liposome membranes containing cholesterol

In cells, BAX pores are described in the OMM but pores in other membranes have not been noted. Specifically, pores in the plasma membrane produce osmotic lysis and necrosis.[59,60] The osmotic lysis of cells would be inconsistent with the apoptotic program of cells, and the molecular basis for this membrane selectivity is important to explaining the physiology of cell death. One of the distinctions between intracellular membranes and the plasma membrane is the high cholesterol composition of the plasma membrane in most cells. Using cholesterol-containing liposomes and mitochondria, we and others observed reduced BAX pore activation.[33] In the preceding section, we have shown that BAX(ΔC19) interaction with membranes involves a rapid but reversible binding to the membrane followed by integration into the membrane, resulting in a very slow dissociation of the integrated protein population from the bilayer. Using surface plasmon resonance, we investigated the effect of cholesterol on the liposome binding and integration of BAX.

The cholesterol-containing liposomes loaded onto the L1 chip similarly to the DOPC:DOPA liposomes and blocked albumin access to the chip surface (see Materials and Methods). The interaction of human BAX(ΔC19) with liposome membranes containing cholesterol is shown in Fig. 8. As with the DOPC:DOPA liposomes, detergent activation of human BAX(ΔC19) was required for significant interaction with the cholesterol-containing membranes. For three preparations of activated BAX(ΔC19), the concentration dependence of binding and membrane integration were determined and averaged (Fig. 8a). Visual inspection of BAX(ΔC19) interaction with DOPC:DOPA:C liposomes indicated that it was distinct from the BAX(ΔC19) interaction with DOPC:DOPA liposomes. The initial membrane association was still rapid and larger for the cholesterol-

Table 1. Analysis of BAX membrane interaction

Type of membrane interaction[a]	K_1 (M)	BAX (mole fraction)[b]	K_2 (M)	BAX (mole fraction)[b]
DOPC:DOPA				
Membrane binding	$2.2\pm0.4\times10^{-6}$	$5.9\pm0.7\times10^{-3}$	$1.37\pm0.45\times10^{-8}$	$0.78\pm0.31\times10^{-3}$
Membrane integration			$2.5\pm0.27\times10^{-7}$	$1.8\pm0.07\times10^{-3}$
DOPC:DOPA:C				
Membrane binding	$1.6\pm1.2\times10^{-6}$	$8.6\pm4.2\times10^{-3}$	$1.4\pm0.46\times10^{-8}$	$1.2\pm0.2\times10^{-3}$
Membrane integration			$1.06\pm0.22\times10^{-8}$	$0.86\pm0.3\times10^{-3}$

[a] As described in the text, the BAX membrane populations were identified by binding and integration with the membrane.
[b] We have used mole fraction to represent membrane-associated BAX populations to allow a direct comparison between experiments as a membrane concentration.[58]

containing membranes. Paradoxically, from this larger pool of membrane-associated BAX, the membrane integration was reduced (Fig. 8b). Analysis of the concentration-dependent membrane association once again demonstrated both low- and high-affinity binding populations as shown in Table 1. The binding pools were approximately 60% larger than those in the DOPC:DOPA liposomes. In spite of this, the integrated fraction was significantly reduced and reached a maximum value that was 58% of that seen in the liposomes without cholesterol. In addition, the ratio of membrane-integrated to membrane-associated BAX demonstrated a very distinct concentration dependence in that there was no increase of the integrated fraction at low concentrations of added BAX (Fig. 8c).

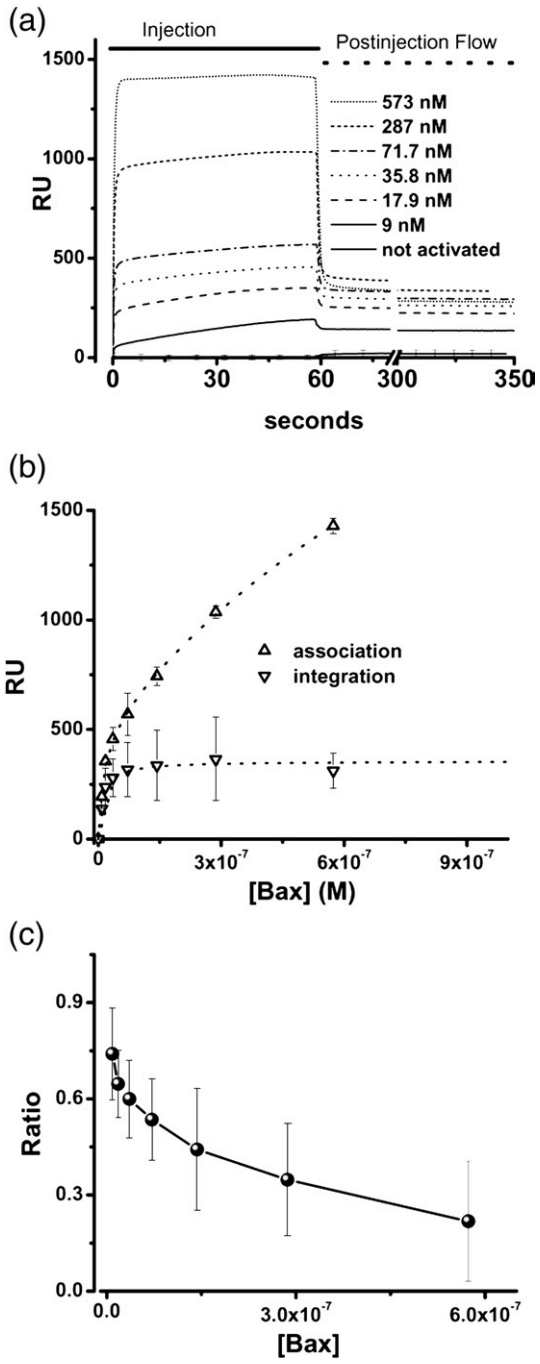

Fig. 8. BAX binding to supported DOPC/DOPA/cholesterol-containing liposomes. The binding and membrane integration of BAX(ΔC19) were studied by surface plasmon resonance using supported liposomes containing cholesterol. (a) BAX(ΔC19) was injected over an L1 chip covered with DOPC:DOPA:C (59:21:20 mol%) liposomes. This protein was prepared as described in Materials and Methods without the use of detergent. Prior to exposure of the BAX(ΔC19) to detergent, the protein did not bind to the liposomes as shown by the open circles (○ ○ ○) at the bottom of the graph that indicate the averaged RU response for the 25–3000 nM BAX(ΔC19) concentration range of unactivated protein. After treatment with detergent, the RU response for the following concentrations is shown: 9 nM (solid), 17.9 nM (dash), 35.8 nM (dot), 71.7 nM (dash–dot), 287 nM (dash–dot–dot), 573 nM (short dash). The injection phase is indicated by the solid line and the wash phase is denoted by the dashed line at the top of the graph. (b) Comparison of membrane-associated (△) and membrane-integrated (▽) protein using the criteria described in the text and calculating the average values and standard deviation as described in Materials and Methods. The dotted lines represent the best fit to an interaction model as described in the text. (c) The ratio of binding and integration of protein plotted as the fraction integrated as concentration of BAX(ΔC19) is increased. Means and standard deviations are computed as described in Materials and Methods.

Discussion

Because BCL-2 family proteins are central arbiters of the mitochondrial mortality decision,[3] we have undertaken a detailed analysis of their biochemical activities. Although 25 genes comprise this family and they generate both pro- and antiapoptotic proteins,[8] apoptosis regulation centers on the activation of a "pore" in the mitochondrial outer membrane by BAX and BAK.[61] We have taken the view that by studying this pore activation in detail, it will become possible to clarify the influences of the regulatory BCL-2 family members. Therefore, we have compared BAX pore activation in liposomes with that activity in mitochondria. Our reconstitution approach permitted a detailed study of the stages of BAX membrane translocation using surface plasmon resonance. This analysis was applied to the mechanism of cholesterol inhibition of BAX pore activation.

A mitochondrial preparation for the study of BAX(ΔC19) pore activation

The *in vivo* death decision polling occurs in the OMM, which has a complex composition of protein and lipid. We have developed a mitochondrial preparation in which to study the translocation and pore-forming activity of BAX protein. Photoconversion of the CF produced deposition of an electron-dense polymeric product in the intermembrane space representing the localization of the CF bet-

ween the inner mitochondrial membrane and OMM.[62] We conclude that the fM preparation is an intact double-membrane mitochondrion having an OMM that provides a diffusion barrier similar to that described for native mitochondria.[39,63,64]

BAX(ΔC19) pore activation in the OMM

Our mitochondrial preparation, fM, satisfied morphologic, metabolic, and OMM functional criteria to be a useful preparation for the study of BAX pore-forming activity. By using the fM preparation, we are able to study the activation of human BAX(ΔC19) in some detail. The pore activation rate and kinetics in mitochondrial and liposome BAX(ΔC19) activity are comparable, as shown in Fig. 4c. The activation of this pore is proposed to be a critical decision point in cell death, with the OMM forming the environment for the BCL-2 family proteins to negotiate this decision.[3,8,65] By using fM, a strong correlation with the pores that we have characterized in defined liposomes is apparent. The specific activity of the purified pore-forming protein is very similar once the necessary correction of the lipid concentration in our assays is considered. Our Hill analysis suggests that the added BAX undergoes a two-stage oligomerization in the membrane that is consistent with our studies in defined liposomes. This comparison suggests that the BAX forms a dimer and tetramer pore in the OMM, a model that is consistent with chemical cross-linking of BAX in the OMM.[12,66]

Effect of cholesterol on BAX pore activation in defined liposomes and mitochondria

Cholesterol is an important component of eukaryotic membranes, having many effects upon membrane characteristics and the activity of membrane components. In beginning these studies, we were attracted by the possibility that the difference in cholesterol content between the plasma membrane and the OMM was an important factor in directing the formation of BAX(ΔC19) pores. Our data and the data of others support this conclusion.[33] Adding cholesterol (≈20 mol%) to liposomes and the OMM significantly inhibits BAX(ΔC19) pore formation. This has more cholesterol than the concentrations reported to be present in the OMM and is less than the cholesterol content of the plasma membranes.[23,31,67,68] Therefore, we conclude that the sterol concentrations of defined liposome membranes can play a role in regulating the pore formation by BAX. To verify that cholesterol was effective in a complex lipid environment, we used liposomes to adjust the cholesterol content of the mitochondrial outer membrane. Direct analysis of the cholesterol content of the fM indicates that the incorporation was successful and produced a cholesterol concentration of ≈20 mol%. Although cholesterol side-chain oxidation can be brisk in isolated mitochondria, this occurs in the inner membrane, whereas outer-membrane cholesterol is quite stable and not oxidized in the isolated organelle.[23] Therefore, our experiments show that the incorporation of exogenous cholesterol into the OMM reduced BAX(ΔC19) pore formation substantially compared with mitochondria fused with liposomes containing only phospholipids. The observation that the cholesterol effect was similar in the simple liposome and the complex mitochondrial membrane environment seems to favor a direct interaction between the sterol and the BAX protein. Direct interactions are also suggested by the putative cholesterol recognition/interaction motif in α-helix 5 (at positions 113–120).[28,69] However, in both liposomes and mitochondria, the *ent*-cholesterol was as effective as the natural compound in reducing BAX pore formation, strongly indicating that cholesterol exerts its effect by influencing the lipid environment and having secondary effects upon BAX pore formation.[20,70] In addition, the reduced pore activation by *ent*-cholesterol at high BAX concentrations in both liposomes and mitochondria may reflect chiral sterol–phospholipid interactions that are reported for the *ent*-cholesterol in phospholipid monolayers.[71]

We conclude that cholesterol could have a significant effect on the mortality decision in cells that are overloaded with this steroid. Mitochondrial cholesterol overload has rarely been studied but has been observed in tumor cell lines[32,72,73] and in cultured cells where mitochondrial cholesterol has been increased pharmacologically.[33] Likewise, cholesterol depletion is reported to enhance apoptosis in statin treatment.[74] However, the mitochondrial membrane environment is complex and steroid oxidation is an active process in these organelles.[23,24] Therefore, when multiple membrane parameters are changed, decreased permeability transition pore activation has also been reported.[34] Our studies have focused on cholesterol in a controlled experimental situation to understand the mechanism by which cholesterol inhibits BAX pore activation.

The interaction of BAX(ΔC19) with liposomes studied by surface plasmon resonance

In order to address the mechanism of cholesterol inhibition of BAX pore activation, we have used surface plasmon resonance to compare the interaction of BAX(ΔC19) with immobilized liposomes (±cholesterol). Surface plasmon resonance has been applied to the study of membrane binding and integration of a number of pore-forming proteins and peptides.[75–79] We have used the attached liposome configuration to quantitatively study the rapid binding of soluble BAX(ΔC19) and concentration-dependent membrane integration of the membrane-bound protein. The data in Fig. 7 clearly demonstrate that the membrane binding of BAX(ΔC19) is completely dependent upon detergent activation of the purified protein. The maximum response to nonactivated BAX(ΔC19) was ≈5 RU, which is consistent with the predicted response from the mass of nonassociated protein [3.3 μM BAX(ΔC19)] injected over the supported liposomes. Therefore,

essentially no membrane association occurs by the nonactivated BAX protein. In cells, BAX also does not associate with the mitochondrial membrane until it is activated.[54,61]

These surface plasmon resonance studies confirm that the interaction of activated BAX with liposome membranes clearly displays the two observed stages of binding and integration.[54] The binding stage is rapid and displays high- and low-affinity components. Membrane integration of BAX is slower but dissociates very slowly, if at all. Analysis of the concentration dependence of binding indicates a high- and a low-affinity population of membrane-associated BAX. The concentration dependence of BAX membrane integration suggests a single population. We plotted the ratio of membrane-integrated to total membrane-associated BAX to study the relationship between these two. In the DOPC/DOPA liposomes, the ratio has an increasing phase, suggesting that binding of BAX to the liposomes enhances the integration step. Membrane binding and integration of BAX saturate even though no protein or typical molecular receptor is present in the membrane. This saturation occurs as the maximum mole fraction (solubility) of the BAX protein associated with the membrane surface or integrated into the membrane is reached. This saturation produces the falling ratio of membrane-integrated to total membrane-associated BAX as higher concentrations of added BAX engage nonproductive modes of membrane association. Interestingly, in the DOPC/DOPA/C membranes, the increasing ratio at low BAX concentration is eliminated. However, since both binding populations are increased in the DOPC/DOPA/C membranes, the integration promoting step and its cholesterol inhibition must occur after the binding steps that we have observed.

Analysis of the cholesterol inhibition of BAX(ΔC19) pore activation

The results of our analysis of BAX association with membranes are presented in Table 1. In this table, the effect of cholesterol on BAX integration into bilayer membranes is apparent. BAX binds to a greater extent (both high- and low-affinity pools are increased by 60%) to membranes that contain cholesterol, but membrane integration is dramatically inhibited (42% reduction). These changes produce the inhibition of BAX pore formation that we observe in liposomes and mitochondria. The effect upon BAX pore activation is consistent with our proposed mechanism of pore activation that includes the in-membrane dimer and tetramer oligomerization of BAX protein. In this model of in-membrane oligomerization, a reduction of membrane integration by cholesterol will suppress pore activation. Cholesterol is known to have a condensing effect upon membranes by reducing the phospholipid area that is especially prominent for the liquid-disordered phase that we have in our DOPC/DOPA liposomes.[52,80] This condensation can be observed as a lateral phase separation in membranes of appropriate composition.[81] Membrane condensation itself could reduce BAX integration without a direct cholesterol–BAX interaction. The equivalence of cholesterol and *ent*-cholesterol inhibition at low BAX integration levels favors membrane condensation over direct sterol–protein interaction. The increased inhibition by *ent*-cholesterol as BAX integration approaches membrane-saturating levels might reflect stereospecific cholesterol interactions with BAX or with membrane phospholipids.[71] If we extrapolate the effect of cholesterol upon the concentration dependence of membrane integration, it appears to explain the inhibition of pore activation. Thus, we have no evidence to suggest stereospecific interaction with the BAX and inhibition of the in-membrane oligomerization steps. However, this does not necessarily contrast with the prior report on effects of cholesterol on BAX.[33] That work compared the BAX integrated to the total membrane-associated protein using trypsin sensitivity. This measure is very similar to the ratio that we calculate, and although we observe that the ratio in DOPC/DOPA/C membranes has a distinct BAX concentration dependence, there is a range where it is similar to that in DOPC/DOPA membranes. Our data only support a cholesterol effect on the membrane integration of BAX that is mediated by altering the membrane environment.

There have now been two investigations showing that the pore-forming activity of BAX is inhibited by cholesterol in liposome membranes. Both of these have increased the cholesterol of the OMM to produce BAX inhibition in that membrane also. By comparison with our results, the cholesterol levels of cell surface membranes will certainly reduce BAX pore formation. It remains to be demonstrated how the cholesterol levels of intracellular membranes change and influence cell death. Resistance of tumor cells to therapy, the persistence and growth of atheromatous lesions and their final rupture, the extent of reperfusion cell death in infarct and stroke regions, and skeletal muscle apoptosis may all be affected by cholesterol levels and the inhibition of BAX activity.

Summary

The 25 BCL-2 family proteins are central regulators of apoptosis. As one of these, BAX is a critical instigator of apoptosis by transitioning from a soluble protein to a membrane-integrated pore. We have characterized this transition in liposomes and human mitochondria. Activation of the soluble protein is required for membrane binding, membrane integration, and in-membrane oligomerization to form pores. Cholesterol is a major inhibitor of BAX pore activation in mitochondria and liposomes. This inhibition does not require direct interaction with the BAX protein but appears to function on the membrane environment to inhibit BAX integration into the membrane bilayer.

Materials and Methods

Preparation of BAX(ΔC19)

Two methods for producing recombinant BAX(ΔC19) were employed. For dequenching experiments, the cDNA for human BAX, with the putative transmembrane carboxy-terminal α-helix truncated, was subcloned into pGEX-KG vector, expressed in BL21(DE3) *Escherichia coli*, and purified as a glutathione *S*-transferase fusion protein. After harvesting by centrifugation, cells were resuspended in lysis buffer [phosphate-buffered saline, pH 7.4, 1% Triton X-100, 1 mM DTT, and Complete Protease Inhibitor Cocktail (Roche, Indianapolis, IN)] and sonicated, and the clarified lysate was applied to glutathione–agarose. Resin was subjected to high salt wash (including 0.1% Triton X-100) and flushed with cleavage buffer [50 mM Tris, pH 7.5, 150 mM NaCl, 0.1% *n*-octyl-β-D-glucopyranoside (OG), 2.5 mM $CaCl_2$, and 1 mM DTT], and BAX(ΔC19) was cleaved from glutathione *S*-transferase tag using thrombin (Novagen, Madison, WI).

For surface plasmon resonance experiments, human BAX(ΔC19) cDNA was subcloned into pTYB1 vector (NEB, Ipswich, MA), expressed in BL21(DE3) *E. coli*, and purified as an intein/chitin-binding domain fusion protein. After harvesting by centrifugation, cells were resuspended in lysis buffer [phosphate-buffered saline, pH 7.4, and Complete Protease Inhibitor Cocktail (Roche)] and sonicated, and clarified lysate was applied to a chitin affinity column. Resin was subjected to high salt wash followed by flushing with cleavage buffer (20 mM Tris, pH 8.0, 500 mM NaCl, 1 mM ethylenediaminetetraacetic acid, and 50 mM DTT) and incubated at 4 °C for 48 h to allow intein self-cleavage and release of recombinant BAX(ΔC19). Eluted proteins were estimated to be >95% pure by Coomassie staining SDS-PAGE gels and stored at 4 °C. BAX(ΔC19) was activated by addition of 2% OG for 1 h at 4 °C and then dialyzed overnight against EB (10 mM Hepes, pH 7.0, 100 mM KCl, and 0.01% NaN_3). BAX(ΔC19) retained pore-forming capacity for >72 h after dialysis with no diminution of activity.

Liposome preparation by reverse-phase method

Liposomes were prepared using the reverse-phase procedure of Szoka and Papahadjopoulos.[82] Lipids were obtained as solutions in chloroform from Avanti Polar Lipids, Inc. (Alabaster, AL). Mixtures of DOPC and DOPA (monosodium salt) and 5-cholestene-3β-ol [cholesterol (C); Sigma-Aldrich, St. Louis, MO] were prepared at a mole fraction ratio of DOPC:DOPA=0.74:0.26 or DOPC:DOPA:C=0.59:0.21:0.20 in chloroform. Chloroform was first evaporated under a stream of N_2 gas and then further removed by vacuum (10^{-5} Torr) for 2 h. Dried lipids were stored in N gas at −20 °C. CF (molecular weight=376) (Molecular Probes, Eugene, OR) was prepared at 20 mM in EB, adjusted to pH 7.2, and stored at 4 °C. Dried lipids were reconstituted by addition of 1 ml ethyl ether and 0.5 ml CF solution. The suspension was sonicated at 1200 W for 20 s, producing a stable suspension, and ether was evaporated on a rotary evaporator at 40 rpm under reduced pressure (water aspiration) for 13 min at room temperature. The 0.5-ml suspension was supplemented with an additional 0.5 ml of the 20-mM CF solution. This mixture was passed through a 22-gauge needle affixed to a mini-extruder (Avanti) containing a 200-nm membrane (Nuclepore, Pleasanton, CA) for three complete cycles. The extravesicular CF was removed by passing the liposome–dye mixture over a 1×20 cm Sephadex G-25-80 (Sigma, St. Louis, MO) column in EB. A liposome peak was collected and analyzed by dynamic light scattering (N5 Submicron Particle Size Analyzer, Beckman Coulter, Fullerton, CA), with a diameter of 207±12.5 nm. Phospholipid concentration in this fraction was determined to be 3.3 mg/ml.[83]

Dequenching analysis of BAX pore activation

We have used the analysis of dequenching to study the activation of pores in bilayer membranes.[19,84–86] Using monodisperse unilamellar vesicles, we studied the activation of membrane pores by measurement of the increased fluorescence as CF exits from the membrane compartment and is diluted into the assay volume. All assays were done at a total lipid concentration of 0.4±0.05 μM. The time dependence of the dequenching from our liposome and mitochondria preparations is well described in Eq. (1), without additional exponential terms.

$$F_{520} = F_0 A_1 (1 - e^{(\text{time}/\tau)}) + m \times \text{time} \quad (1)$$

The formation of a 10- to 30-Å pore in a 200-nm vesicle (or mitochondrion, see Fig. 2) will permit the equilibration of CF with the media within 30–100 ms.[87,88] In the timescale of our assay, a single pore opening will not be resolved and the exponential dequenching we observe represents the kinetics of pore activation. A linear component in the time series was frequently not observed but represents pores that are unstable and which close before single vesicle dequenching is complete with subsequent pore activation being required to complete dequenching.[89] For a time-series experiment, the fractional dequenching at each time point was determined by normalizing the fluorescence (Fl) with the Triton X-100-generated total dequenching for each assay [Eq. (2)].

$$F_{520} = \frac{\text{Fl}_{\text{time}} - \text{Fl}_{\text{baseline}}}{\text{Fl}_{\text{Triton X100}} - \text{Fl}_{\text{baseline}}} \quad (2)$$

The analysis of BAX pore activation was undertaken by determining the time constant, τ, and the total exponential fluorescence change, A_1, for each time-series dequenching. The kinetic constants were determined by nonlinear least-squares analysis using the Levenberg–Marquardt algorithm, which yielded χ^2 values of <0.001 for each time series.

Assessment of BAX(ΔC19)–liposome interaction by centrifugation and silver staining

OG-activated BAX(ΔC19) was dialyzed overnight against EB. BAX was applied to liposomes±cholesterol (1.1 μM total lipid concentration), incubated for 10 min at room temperature, and ultracentrifuged at 150,000*g* for 20 min at 4 °C. The supernatant was collected and the proteoliposome pellet was subjected to alkaline extraction by resuspension in 100 mM sodium carbonate for 30 min on ice. Samples were again ultracentrifuged and supernatant and pellet fractions were collected. After SDS-PAGE and silver staining, relative intensities of BAX bands were quantified using QuantityOne software (Bio-Rad, Hercules, CA).

Preparation of mitochondria

Mitochondria were prepared from cultured cells following published procedures.[90,91] The mitochondria were isolated from HeLa cells maintained in culture where the unstimulated rate of apoptosis is <5%. We used 250 mM

sucrose for osmotic stabilization (pH 7.0, 10 mM Hepes) and added 1 mM EGTA to maintain low Ca^{2+}. All procedures were performed at 4 °C on ice baths except as noted. Cell cultures were washed with ice-cold sucrose solution to remove media and serum, and the cells were mechanically scraped from the dishes. After homogenization (40 strokes with a loose Dounce), the nuclei and undisrupted cells were removed by centrifugation at 500*g*. Mitochondria were then collected by centrifugation at 9000*g*. The mitochondrial pellet was resuspended, and protein concentration was determined using the Micro BCA Protein Assay Kit (Pierce Chemical Co., Rockford, IL). The mitochondria were suspended at 1 mg/ml protein in the unilamellar liposome preparation for fusion as described previously.[39,40] The CF-loaded liposomes were 1 mM in lipid and contained 2×10^{12} liposomes/ml. The mitochondria and liposomes were incubated together at 15 °C for 60 min and then the pH dropped to 6.5 by addition of 60 μl of 100 mM Pipes (pH 6) for 5 min. The fM were pelleted at 9000*g* and washed two further times in 250 mM sucrose buffer to remove unfused liposomes. Lipid analysis by Dr. Richard Gross of the Department of Medicine at Washington University allowed us to adjust the fusion protocol in order to incorporate the desired amount of cholesterol into the mitochondria. This analysis showed that the liposome fusion increased DOPA to three times the DOPA in the isolated mitochondria before fusion.[92] We used this ratio to calculate the OMM cholesterol concentration, which increased to 16±0.4 mol%, when we were using liposomes containing 20 mol% cholesterol. Cholesterol in liposome and mitochondria preparations was converted to trimethylsilyl ethers and determined using gas chromatography–mass spectrometry by Dr. Dan Ory of the Department of Medicine, Washington University School of Medicine.[93] Mitochondria fused to these levels were used in all of the experiments to test the effect of cholesterol on BAX activity in mitochondria.

Electron microscopy and photoconversion of the mitochondrial preparations

Mitochondria were purified as above and fixed with 2.5% glutaraldehyde in 0.1 M sodium cacodylate for 30 min on ice, after which they were spun at top speed in a tabletop microfuge to form a tight pellet. After rinsing, the pellet was sequentially stained with osmium tetroxide and uranyl acetate and then dehydrated and embedded in Polybed 812. Tissue was thin sectioned on a Reichert–Jung Ultracut, viewed on a Zeiss 902 electron microscope, and recorded with Kodak E.M. film. For photoconversion, the mitochondria were washed after fixation and treated with 6 mM potassium cyanide and then suspended in cacodylate buffer with 2.8 mM 3,3′-diaminobenzidine tetrahydrochloride for exposure to a 75-W xenon lamp. After 6 min, the mitochondria are washed by centrifugation and processed for electron microscopy as above.

Measurement of mitochondrial oxygen consumption

Mitochondria were prepared as described above. Mitochondria at a protein concentration of ≈1 mg/ml were placed into the Instech dissolved oxygen measuring system (Warner Instruments, Hamden, CT) in 150 mM KCl (pH 7.0), 1 mM EGTA, and 5 mM DTT at 20 °C. The buffer was equilibrated with 95% O_2 and stored in an airtight syringe prior to use. The concentration of dissolved O_2 was corrected for atmospheric pressure. During the assay, the mitochondria were sequentially treated with 5 mM malate, 5 mM ADP, 2 μM rotenone, 5 mM succinate, 10 mM ascorbate, and *N*,*N*,*N*,*N*-tetramethyl-*p*-phenylenediamine (TMPD) and a baseline obtained in 10 mM azide. After the addition of ascorbate–TMPD, the rate of oxygen consumption was dependent upon site IV, which employs cytochrome *c* and cytochrome oxidase in the transfer of electrons to molecular oxygen.[94] The rates of oxygen consumption were normalized for protein concentration.

Planar lipid bilayer studies on isolated fM

Planar lipid bilayers were prepared from the phospholipids DOPC:DOPA (74:26 mol%). Phospholipids were obtained from Avanti Polar lipids in chloroform solution and were mixed to the correct ratio, and the chloroform was removed under nitrogen. The lipids were then stored under nitrogen at −20 °C until dissolved in decane at 20 mg/ml. Briefly, 2 μl of lipid solution was applied to 0.25 mm orifice of a polystyrene cuvette (Warner Instruments), and the solvent was allowed to evaporate. The cuvette was then placed into a bilayer chamber and connected to a bilayer clamp (BC525-c; Warner Instruments) by Ag/AgCl electrodes via agar bridges. Data were collected using CLAMPEX 9.0 (Axon Instruments, Foster City, CA), archived on videotape using a Neurocorder DR-484 (Neuro Data Instruments, Delaware Water Gap, PA), and analyzed using Origin (OriginLab Corporation, Northampton, MA) and CLAMPFIT (Axon Instruments). Bilayers were formed by spreading with a polished glass rod and allowed to thin to a capacitance of 0.4 $\mu F/cm^2$, at which point the noise was typically 0.2 pA and the leak conductance was 2 pS. The salt concentrations are described in the appropriate figure legends. Outward (positive) currents were defined as K^+ moving *cis* to *trans*. All solutions were buffered to pH 7.0 with 10 mM K-Hepes. Mitochondria (10 μg of protein) were added to the *cis* chamber with mixing. To vary calcium concentration, we added EGTA and $CaCl_2$ as indicated. The MilliQ water employed for buffers in these studies averaged 30 μM Ca^{2+}, and mitochondrial isolation buffer contained 1 mM EGTA to reduce free Ca^{2+} to <1 μM. Calcium was varied by adding 100 μM $CaCl_2$ or 100 μM EGTA to the bilayer chamber.

Surface plasmon resonance studies of BAX–liposome interaction

These studies were done using Biacore X instrumentation and software (Biacore Division of GE Healthcare, Uppsala, Sweden) at an ambient temperature of 20 °C. Buffers were filtered through 0.22 μm filter prior to use. Liposomes were prepared as described above. The buffer was EB unless noted. The sensor surface of an L1 chip (Biacore) was equilibrated in EB. Liposomes were injected at a phospholipid concentration of 0.6 mg/ml across the sensor surface at a flow rate of 3 μl/min for 12 min. Loosely associated liposomes were washed from the surface by increasing the flow rate of running buffer to 500 μl/min for 30 s. Bovine serum albumin (1 mg/ml) was injected at 15 μl/min for 2 min to ascertain the extent of liposome coverage of the surface and to block remaining nonspecific binding sites.[58] The DOPC:DOPA liposomes loaded to 13±0.9 ng lipid/μm^2 and the DOPC:DOPA:C liposomes loaded to 12.3±1.2 ng lipid/μm^2. Variation in loading was primarily due to variation in the liposome size distribution. BAX(ΔC19) protein was injected over supported liposomes at 30 μl/min, and the dissociation was

observed for 5 min at the same flow rate at which the protein was injected. The response was corrected for injection artifacts. Data were analyzed and displayed using BIAevaluation (Biacore) and Origin 7.5 (OriginLab Corporation) software. At each concentration of BAX protein, the line presented results from the averaging of two to four independent binding studies. The standard deviation from this averaging is shown in the binding plots when its value is larger than the symbols or line that is being displayed.

References

1. Steller, H. (1995). Mechanisms and genes of cellular suicide. *Science*, **267**, 1445–1449.
2. Adams, J. M. & Cory, S. (2007). BCL-2-regulated apoptosis: mechanism and therapeutic potential. *Curr. Opin. Immunol.* **19**, 1–9.
3. Danial, N. N. & Korsmeyer, S. J. (2004). Cell death: critical control points. *Cell*, **116**, 205–219.
4. Korsmeyer, S. J., Wei, M. C., Saito, M., Weiler, S., Oh, K. J. & Schlesinger, P. H. (2000). Pro-apoptotic cascade activates BID, which oligomerizes BAK or BAX into pores that result in the release of cytochrome *c*. *Cell Death Differ.* **7**, 1166–1173.
5. Dejean, L. M., Martinez-Caballero, S. & Kinnally, K. W. (2006). Is mac the knife that cuts cytochrome *c* from mitochondria during apoptosis? *Cell Death Differ.* **13**, 1–9.
6. Green, D. R. & Kroemer, G. (2004). The pathophysiology of mitochondrial cell death. *Science*, **305**, 626–629.
7. Jiang, X. & Wang, X. (2004). Cytochrome *c*-mediated apoptosis. *Annu. Rev. Biochem.* **73**, 87–106.
8. Reed, J. C. (2006). Proapoptotic multidomain BCL-2/BAX-family proteins: mechanisms, physiological roles, and therapeutic opportunities. *Cell Death Differ.* **13**, 1378–1386.
9. Youle, R. J. (2007). Cellular demolition and the rules of engagement. *Science*, **315**, 776–777.
10. Leber, B., Lin, J. & Andrews, D. W. (2007). Embedded together: the life and death consequences of interaction of the BCL-2 family with membranes. *Apoptosis*, **12**, 897–911.
11. Annis, M. G., Soucie, E. L, Dlugosz, P. J., Cruz-Aguado, J. A, Penn, L. Z., Leber, B. & Andrews, D. W. (2005). BAX forms multispanning monomers that oligomerize to permeabilize membranes during apoptosis. *EMBO J.* **24**, 2096–2103.
12. Mikhailov, V., Mikhailova, M., Degenhardt, K., Venkatachalam, M. A., White, E. & Saikumar, P. (2003). Association of BAX and Bak homo-oligomers in mitochondria: BAX requirement for Bak reorganization and cytochrome *c* release. *J. Biol. Chem.* **278**, 5367–5376.
13. Mikhailov, V., Mikhailova, M., Pulkrabek, D. J., Dong, Z., Venkatachalam, M. A. & Saikumar, P. (2001). BCL-2 prevents BAX oligomerization in the mitochondrial outer membrane. *J. Biol. Chem.* **276**, 18361–18374.
14. Gross, A., Jockel, J., Wei, M. C. & Korsmeyer, S. J. (1998). Enforced dimerization of BAX results in its translocation, mitochondrial dysfunction and apoptosis. *EMBO J.* **17**, 3878–3885.
15. Uren, R. T., Dewson, G., Chen, L., Coyne, S. C., Huang, D. C. S., Adams, J. M. & Kluck, R. M. (2007). Mitochondrial permeabilization relies on BH3 ligands engaging multiple prosurvival BCL-2 relatives, not Bak. *J. Cell Biol.* **177**, 277–287.
16. Willis, S. N., Fletcher, J. I., Kaufmann, T., van Delft, M. F., Chen, L., Czabotar, P. E. *et al.* (2007). Apoptosis initiated when BH3 ligands engage multiple BCL-2 homologs, not BAX or Bak. *Science*, **315**, 856–859.
17. Kim, H., Rafiuddin-Shah, M., Tu, H. C., Jeffers, J. R., Zambetti, G. P., Hsieh, J. J. & Cheng, E. H. (2006). Hierarchical regulation of mitochondrion-dependent apoptosis by BCL-2 subfamilies. *Nat. Cell Biol.* **8**, 1348–1358.
18. Schlesinger, P. H., Gross, A., Xin, X. M., Yamamoto, K., Saito, M., Waksman, G. & Korsmeyer, S. J. (1997). Comparison of the ion channel characteristics of pro apoptotic BAX and anti-apoptotic BCL-2. *Proc. Natl Acad. Sci. USA*, **94**, 11357–11362.
19. Saito, M., Korsmeyer, J. & Schlesinger, H. (2000). BAX dependent cytochrome-*c* transport reconstituted in pure liposomes. *Nat. Cell Biol.* **2**, 553–555.
20. Westover, E. J. & Covey, D. F. (2004). The enantiomer of cholesterol. *J. Membr. Biol.* **202**, 61–72.
21. Mouritsen, O. G. & Zuckermann, M. J. (2004). What's so special about cholesterol? *Lipids*, **39**, 1101–1113.
22. Soccio, R. E. & Breslow, J. L. (2004). Intracellular cholesterol transport. *Arterioscler., Thromb., Vasc. Biol.* **24**, 1150–1160.
23. Cheng, B., Hsu, D. K. & Kimura, T. (1985). Utilization of intramitochondrial membrane cholesterol by cytochrome P-450-dependent cholesterol side-chain cleavage reaction in bovine adrenocortical mitochondria: steroidogenic and non-steroidogenic pools of cholesterol in the mitochondrial inner membranes. *Mol. Cell. Endocrinol.* **40**, 233–243.
24. Tuckey, R. C., Headlam, M. J., Bose, H. S. & Miller, W. L. (2002). Transfer of cholesterol between phospholipid vesicles mediated by the steroidogenic acute regulatory protein (StAR). *J. Biol. Chem.* **277**, 47123–47128.
25. Leonarduzzi, G., Biasi, F., Chiarpotto, E. & Poli, G. (2004). Trojan horse-like behavior of a biologically representative mixture of oxysterols. *Mol. Aspects Med.* **25**, 155–167.
26. Lacapere, J. J. & Papadopoulos, V. (2003). Peripheral-type benzodiazepine receptor: structure and function of a cholesterol-binding protein in steroid and bile acid biosynthesis. *Steroids*, **68**, 569–585.
27. Casellas, P., Galiegue, S. & Basile, A. S. (2002). Peripheral benzodiazepine receptors and mitochondrial function. *Neurochem. Int.* **40**, 475–486.
28. Jamin, N., Neumann, J.-M., Ostuni, M. A., Ngoc Vu, T. K., Yao, Z.-X., Murail, S. *et al.* (2005). Characterization of the cholesterol recognition amino acid consensus sequence of the peripheral-type benzodiazepine receptor. *Mol. Endocrinol.* **19**, 588–594.
29. Russell, D. W. (2000). Oxysterol biosynthetic enzymes. *Biochim. Biophys. Acta*, **1529**, 126–135.
30. Omura, T. (2006). Mitochondrial P450s. *Chem.-Biol. Interact.* **163**, 86–93.
31. Feo, F., Canuto, R. A., Bertone, G., Garcea, R. & Pani, P. (1973). Cholesterol and phospholipid composition of mitochondria and microsomes isolated from morris hepatoma 5123 and rat liver. *FEBS Lett.* **33**, 229–333.
32. Campbell, A. M. & Chan, S. H. P. (2007). The voltage dependent anion channel affects mitochondrial cholesterol distribution and function. *Arch. Biochem. Biophys.* **466**, 203–210.
33. Lucken-Ardjomande, S., Montessuit, S. & Martinou, J.-C. (2007). BAX activation and stress-induced apoptosis delayed by the accumulation of cholesterol in mitochondrial membranes. *Cell Death Differ.* **15**, 484–493.
34. Martinez-Abundis, E., Garcia, N., Correa, F., Franco, M. & Zazueta, C. (2007). Changes in specific lipids regulate BAX-induced mitochondrial permeability transition. *FEBS J.* **274**, 6500–6510.

35. Chen, C., Cui, J., Lu, H., Wang, R., Zhang, S. & Shen, P. (2007). Modeling of the role of a BAX-activation switch in the mitochondrial apoptosis decision. *Biophys. J.* **92**, 4304–4315.
36. Er, E., Oliver, L., Cartron, P.-F., Juin, P., Manon, S. & Vallette, M. (2006). Mitochondria as the target of the pro-apoptotic protein BAX. *Biochim. Biophys. Acta*, **1757**, 1301–1311.
37. Cartron, P.-F., Arokium, H., Oliver, L., Meflah, K., Manon, S. & Vallette, M. (2005). Distinct domains control the addressing and the insertion of BAX into mitochondria. *J. Biol. Chem.* **280**, 10587–10598.
38. Kroemer, G., Galluzzi, L. & Brenner, C. (2007). Mitochondrial membrane permeabilization in cell death. *Physiol. Rev.* **87**, 99–163.
39. Cortese, J. D., Voglino, A. L. & Hackenbrock, C. R. (1991). Ionic strength of the intermembrane space of intact mitochondria as estimated with fluorescein–BSA delivered by low pH fusion. *J. Cell Biol.* **113**, 1331–1340.
40. Gupte, S. S. & Hackenbrock, C. R. (1988). The role of cytochrome *c* diffusion in mitochondrial electron transport. *J. Biol. Chem.* **263**, 5248–5253.
41. Schikorski, T. & Stevens, C. F. (2001). Morphological correlates of functionally defined synaptic vesicle populations. *Nat. Neurosci.* **4**, 391–395.
42. Deerinck, T. J., Martone, M. E., Lev-Ram, V., Green, D. P., Tsien, R. Y., Spector, D. L. *et al.* (1994). Fluorescence photooxidation with eosin: a method for high resolution immunolocalization and in situ hybridization detection for light and electron microscopy. *J. Cell Biol.* **126**, 901–910.
43. Komarov, A. G., Deng, D., Craigen, W. J. & Colombini, M. (2005). New insights into the mechanism of permeation through large channels. *Biophys. J.* **89**, 3950–3959.
44. Hulbert, A. J., Turner, N., Hinde, J., Else, P. & Guderley, H. (2006). How might you compare mitochondria from different tissues and different species? *J. Comp. Physiol., B.* **176**, 93–105.
45. Bathori, G., Csordas, G., Garcia-Perez, C., Davies, E. & Hajnoczky, G. (2006). Ca^{2+}-dependent control of the permeability properties of the mitochondrial outer membrane and voltage-dependent anion-selective channel (VDAC). *J. Biol. Chem.* **281**, 17347–17358.
46. Pavlov, E., Grigoriev, S. M., Dejean, L. M., Zweihorn, C. L., Mannella, C. A. & Kinnally, K. W. (2005). The mitochondrial channel VDAC has a cation-selective open state. *Biochim. Biophys. Acta*, **1716**, 96–102.
47. Rostovtseva, T. & Colombini, M. (1997). VDAC channels mediate and gate the flow of ATP: implications for the regulation of mitochondrial function. *Biophys. J.* **72**, 1954–1962.
48. Rostovtseva, T. K., Tan, W. & Colombini, M. (2005). On the role of VDAC in apoptosis: fact and fiction. *J. Bioenerg. Biomembr.* **37**, 129–142.
49. Schein, S. J., Colombini, M. & Finkelstein, A. (1976). Reconstitution in planar lipid bilayers of a voltage-dependent anion-selective channel obtained from paramecium mitochondria. *J. Membr. Biol.* **30**, 99–120.
50. Scorrano, L., Oakes, S. A., Opferman, J. T., Cheng, E. H., Sorcinelli, M. D., Pozzan, T. & Korsmeyer, S. J. (2003). BAX and BAK regulation of endoplasmic reticulum Ca^{2+}: a control point for apoptosis. *Science*, **300**, 135–139.
51. Feigenson, G. W. (2007). Phase boundaries and biological membranes. *Annu. Rev. Biophys. Biomol. Struct.* **36**, 63–77.
52. Hung, W. C., Lee, M. T., Chen, F. Y. & Huang, H. W. (2007). The condensing effect of cholesterol in lipid bilayers. *Biophys. J.* **92**, 3960–3967.
53. Smaby, J. M., Momsen, M. M., Brockman, H. L. & Brown, R. E. (1997). Phosphatidylcholine acyl unsaturation modulates the decrease in interfacial elasticity induced by cholesterol. *Biophys. J.* **73**, 1492–1505.
54. Goping, I. S., Gross, A., Lavoie, J. N., Nguyen, M., Jemmerson, R., Roth, K. *et al.* (1998). Regulated targeting of BAX to mitochondria. *J. Cell Biol.* **143**, 207–215.
55. Wolter, K. G., Hsu, Y.-T., Smith, C. L., Nechushtan, A., Xi, X.-G. & Youle, R. J. (1997). Movement of BAX from the cytosol to mitochondria during apoptosis. *J. Cell Biol.* **139**, 1281–1292.
56. Cho, W. & Stahelin, R. V. (2005). Membrane–protein interactions in cell signaling and membrane trafficking. *Annu. Rev. Biophys. Biomol. Struct.* **34**, 119–151.
57. Erb, E.-M., Chen, X., Allen, S., Roberts, C. J., Tendler, S. J. B., Davies, M. C. & Forsen, S. (2000). Characterization of the surfaces generated by liposome binding to the modified dextran matrix of a surface plasmon resonance sensor chip. *Anal. Biochem.* **280**, 29–35.
58. Anderluh, G., Besenicar, M., Kladnik, A., Lakey, J. H. & Macek, P. (2005). Properties of nonfused liposomes immobilized on an L1 Biacore chip and their permeabilization by a eukaryotic pore-forming toxin. *Anal. Biochem.* **344**, 43–52.
59. Shaposhnikova, V. V., Egorova, M. V., Kudryavtsev, A. A., Levitman, M. K. & Korystov, Y. N. (1997). The effect of melittin on proliferation and death of thymocytes. *FEBS Lett.* **410**, 285–288.
60. Ownby, C. L., Powell, J. R., Jiang, M. S. & Fletcher, J. E. (1997). Melittin and phospholipase A2 from bee (*Apis mellifera*) venom cause necrosis of murine skeletal muscle *in vivo*. *Toxicon*, **35**, 67–80.
61. Youle, R. J. & Strasser, A. (2008). The BCL-2 protein family: opposing activities that mediate cell death. *Nat. Rev., Mol. Cell Biol.* **9**, 47–59.
62. Harata, N., Ryan, T. A., Smith, S. J., Buchanan, J. & Tsien, R. W. (2001). Visualizing recycling synaptic vesicles in hippocampal neurons by FM 1–43 photoconversion. *Proc. Natl Acad. Sci. USA*, **98**, 12748–12753.
63. Rostovtseva, T. K., Kazemi, N., Weinrich, M. & Bezrukov, S. M. (2006). Voltage gating of vdac is regulated by nonlamellar lipids of mitochondrial membranes. *J. Biol. Chem.* **281**, 37496–37506.
64. Cortese, J. D. & Hackenbrock, C. R. (1993). Motional dynamics of functional cytochrome *c* delivered by low pH fusion into the intermembrane space of intact mitochondria. *Biochim. Biophys. Acta*, **1142**, 194–202.
65. Willis, S. N. & Adams, J. M. (2005). Life in the balance: how BH3-only proteins induce apoptosis. *Curr. Opin. Cell Biol.* **17**, 617–625.
66. Cheng, E. H.-Y., Sheiko, T. V., Fisher, J. K., Craigen, W. J. & Korsmeyer, S. J. (2003). VDAC2 inhibits BAK activation and mitochondrial apoptosis. *Science*, **301**, 513–517.
67. Rouslin, W., MacGee, J., Gupte, S., Wesselman, A. & Epps, D. E. (1982). Mitochondrial cholesterol content and membrane properties in porcine myocardial ischemia. *Am. J. Physiol.* **242**, H254–H259.
68. Hauser, H. & Poupart, G. (2005). The Structure of Biological Membranes, pp. 1–53, 2nd edit. CRC Press, Boca Raton, FL.
69. Epand, R. M. (2006). Cholesterol and the interaction of proteins with membrane domains. *Prog. Lipid Res.* **45**, 279–294.
70. Crowder, C. M., Westover, E. J., Kumar, A. S., Jr, Ostlund, R. E. & Covey, D. F. (2001). Enantiospecificity of cholesterol function *in vivo*. *J. Biol. Chem.* **276**, 44369–44372.
71. Alakoskela, J.-M., Sabatini, K., Jiang, X., Laitala, V., Covey, D. F. & Kinnunen, P. K. J. (2008). On

enantiospecific interactions between cholesterol and phospholipids. *Langmuir*, **24**, 830–836.
72. Grain, R. C., Clark, R. W. & Harvey, B. E. (1983). Role of lipid transfer proteins in the abnormal lipid content of morris hepatoma mitochondria and microsomes. *Cancer Res.* **43**, 3197–3202.
73. Graham, J. M. & Green, C. (1970). The properties of mitochondria enriched *in vitro* with cholesterol. *Eur. J. Biochem.* **12**, 58–66.
74. Werner, M., Sacher, J. & Hohenegger, M. (2004). Mutual amplification of apoptosis by statin-induced mitochondrial stress and doxorubicin toxicity in human rhabdomyosarcoma cells. *Br. J. Pharmacol.* **143**, 715–724.
75. Anderluh, G., Maceka, P. & Lakey, J. H. (2003). Peeking into a secret world of pore-forming toxins: membrane binding processes studied by surface plasmon resonance. *Toxicon*, **42**, 225–228.
76. Bavdek, A., Gekara, N. O., Priselac, D., Aguirre, I. G., Darji, A., Chakraborty, T. *et al.* (2007). Sterol and pH interdependence in the binding, oligomerization, and pore formation of Listeriolysin O. *Biochemistry*, **46**, 4425–4437.
77. Bastos, M., Bai, G., Gomes, P., Andreu, D., Goormaghtigh, E. & Prieto, M. (2007). Energetics and partition of two cecropin–melittin hybrid peptides to model membranes of different composition. *Biophys. J.* **94**, 2128–2141.
78. Besenicar, M., Macek, P., Lakey, J. H. & Anderluh, G. (2006). Surface plasmon resonance in protein–membrane interactions. *Chem. Phys. Lipids.* **141**, 169–178.
79. Papo, N. & Shai, Y. (2003). Exploring peptide membrane interaction using surface plasmon resonance: differentiation between pore formation versus membrane disruption by lytic peptides. *Biochemistry*, **42**, 458–466.
80. Ali, S., Smaby, J. M., Brockman, H. L. & Brown, R. E. (1994). Cholesterol's interfacial interactions with galactosylceramides. *Biochemistry*, **33**, 2900–2906.
81. McConnell, H. M. & Vrljic, M. (2003). Liquid–liquid immiscibility in membranes. *Annu. Rev. Biophys. Biomol. Struct.* **32**, 469–492.
82. Szoka, F. & Papahadjopoulos, D. (1978). Procedure for preparation of liposomes with large internal aqueous space and high capture by reverse-phase evaporation. *Proc. Natl Acad. Sci. USA*, **75**, 4194–4198.
83. Stewart, J. C. M. (1980). Colorimetric determination of phospholipids with ammonium ferrothiocyanate. *Anal. Biochem.* **104**, 10–14.
84. Schlesinger, P. H. & Saito, M. (2006). The BAX pore in liposomes, biophysics. *Cell Death Differ.* **13**, 1403–1408.
85. Gokel, G. W., Schlesinger, P. H., Djedovic, N. K., Ferdani, R., Harder, E. C., Hu, J. *et al.* (2004). Functional, synthetic organic chemical models of cellular ion channels. *Bioorg. Med. Chem.* **12**, 1291–1304.
86. Djedovic, N., Ferdani, R., Harder, E., Pajewska, J., Pajewski, R., Weber, M. E. *et al.* (2005). The C- and N-terminal residues of synthetic heptapeptide ion channels influence transport efficacy through phospholipid bilayers. *New J. Chem.* **29**, 291–305.
87. Miller, C. (1984). Ion channels in liposomes. *Annu. Rev. Physiol.* **46**, 549–558.
88. Hille, B. (2001). Ionic Channels of Excitable Membranes, Chapter 11, pp. 347–376, 3rd edit. Sinuaer Associates Inc., Sunderland, MA.
89. Rex, S. & Schwarz, G. (1998). Quantitative studies on the melittin-induced leakage mechanism of lipid vesicles. *Biochemistry*, **37**, 2336–2345.
90. Pallotti, F. & Lenaz, G. (2001). Mitochondria and mitoplasts from cultured cells. In *Methods in Cell Biology* (Pon, L. A. & Schon, E. A., eds), vol. 65, pp. 4–31. Academic Press, Burlington, MA.
91. Frezza, C., Cipolat, S. & Scorrano, L. (2007). Organelle isolation: functional mitochondria from mouse liver, muscle and cultured fibroblasts. *Nat. Protoc.* **2**, 287–295.
92. Mancuso, D. J., Sims, H. F., Han, X., Jenkins, C. M., Guan, S. P., Yang, K. *et al.* (2007). Genetic ablation of calcium-independent phospholipase A2gamma leads to alterations in mitochondrial lipid metabolism and function resulting in a deficient mitochondrial bioenergetic phenotype. *J. Biol. Chem.* **282**, 34611–34622.
93. Frolov, A., Zielinski, S. E., Crowley, J. R., Dudley-Rucker, N., Schaffer, J. E. & Ory, D. S. (2003). NPC1 and NPC2 regulate cellular cholesterol homeostasis through generation of low density lipoprotein cholesterol-derived oxysterols. *J. Biol. Chem.* **278**, 25517–25525.
94. Nicholls, D. G. & Ferguson, S. J. (2001). Bioenergetics 3, Chapter 5: Respiratory Chains, pp. 89–154, Academic Press, London, UK.